J. Fluid Mech. (2017), *vol.* 818, *pp.* 319–343.
doi:10.1017/jfm.2017.99

Short-wavelength local instabilities of a circular Couette flow with radial temperature gradient

Oleg N. Kirillov[1,2,†] **and Innocent Mutabazi**[3]

[1]Northumbria University, Newcastle upon Tyne, NE1 8ST, UK

[2]Steklov Mathematical Institute, Russian Academy of Sciences, Gubkina 8, Moscow 119991, Russia

[3]Laboratoire Ondes et Milieux Complexes (LOMC), UMR 6294, CNRS-Université du Havre, Normandie Université, B.P. 540, 76058 Le Havre CEDEX, France

(Received 11 June 2016; revised 10 February 2017; accepted 13 February 2017)

We perform a linearized local stability analysis for short-wavelength perturbations of a circular Couette flow with a radial temperature gradient. Axisymmetric and non-axisymmetric perturbations are considered and both the thermal diffusivity and the kinematic viscosity of the fluid are taken into account. The effect of asymmetry of the heating both on centrifugally unstable flows and on the onset of instabilities of centrifugally stable flows, including flows with a Keplerian shear profile, is thoroughly investigated. It is found that an inward temperature gradient destabilizes the Rayleigh-stable flow either via Hopf bifurcation if the liquid is a very good heat conductor or via steady state bifurcation if viscosity prevails over the thermal conductance.

Key words: buoyancy-driven instability, convection in cavities, rotating flows

1. Introduction

Circular Couette flow of a viscous Newtonian fluid between two coaxial differentially rotating cylinders is a canonical system for modelling instabilities leading to spatio-temporal patterns and transition to turbulence in many natural and industrial processes. Modern astrophysical applications require understanding of basic instability mechanisms in rotating flows with the Keplerian shear profile in accretion- and protoplanetary disks that are hydrodynamically stable according to the centrifugal Rayleigh criterion. Usually, these instabilities are a consequence of additional factors such as electrical conductivity of the fluid and the magnetic field of the central gravitating object (Chandrasekhar 1961; Lifshitz 1987; Friedlander & Vishik 1995; Urpin & Brandenburg 1998; Kucherenko & Kryvko 2013; Kirillov, Stefani & Fukumoto 2014; Child, Kersalé & Hollerbach 2015; Balbus & Potter 2016). However, in the so-called ‘dead-zones’ of protoplanetary disks that are characterized by high electrical resistivity due to very low ionization levels, some magnetohydrodynamic (MHD) instabilities become inefficient (e.g. the standard Velikhov–Chandrasekhar magnetorotational instability (MRI) in an axial magnetic field). Alternative mechanisms include MRIs caused by azimuthal or helical magnetic

† Email address for correspondence: oleg.kirillov@northumbria.ac.uk

fields that work well also in the inductionless limit at a very low conductivity (Kirillov & Stefani 2013; Kirillov *et al.* 2014) as well as pure hydrodynamic finite-amplitude nonlinear instabilities (Marcus *et al.* 2013). Some recent studies indicated a possibility that Keplerian disks with strong mean radial temperature gradients can support the so-called Goldreich–Schubert–Fricke (GSF) instability, which is the instability of short-radial-wavelength inertial modes (Economides & Moir 1980; Urpin & Brandenburg 1998; Nelson, Gressel & Umurhan 2013; Balbus & Potter 2016). These astrophysical implications renewed interest in the effect of radial temperature gradients on the stability of circular Couette flow and its observation in the laboratory (Yoshikawa, Nagata & Mutabazi 2013; Meyer, Yoshikawa & Mutabazi 2015).

Typically, instabilities in circular Couette flow are studied numerically, for instance, via normal mode analysis or direct numerical simulations. An alternative technique developed in the literature (Eckhoff 1981; Lifshitz 1987; Lifschitz 1991; Lifschitz & Hameiri 1991; Dobrokhotov & Shafarevich 1992; Lifschitz & Hameiri 1993; Eckhardt & Yao 1995; Friedlander & Vishik 1995) is based on perturbations of a background flow in a small parameter, representing a short wavelength, as in geometric optics (Lifschitz, Suters & Beale 1996). These perturbations are localized wave envelopes moving along the trajectories of fluid elements. The flow is unstable if the amplitude of the envelope demonstrates an unbounded growth in time along at least one trajectory.

The geometric optics stability analysis requires the representation of the solution to the governing equations linearized about the background flow as a generalized progressive wave expansion (Eckhoff 1981). Since the leading-order term in this expansion dominates the solution for a sufficiently long time, provided that the short-wavelength parameter is small enough, it is sufficient for detecting instability to determine the growth rate of the lowest-order amplitude (Eckhoff 1981; Lifschitz 1991). The growth rates are given by the real parts of the roots of the dispersion relation of the linear transport equation for the lowest-order amplitude that depends on the wave vector of the perturbation. The wave vector evolves along a stream line of the flow and this evolution is governed by an eikonal equation. The stream line passing through a particular point fulfils a corresponding trajectory equation. Thus, detecting instabilities localized near a particular fluid element location, moving with the flow, reduces to solving a system of ordinary differential equations for the wave vector and amplitude, along particle paths in the underlying flow, with coefficients depending on the unperturbed velocity field (Lifschitz *et al.* 1996).

The geometric optics stability analysis has proved successful in solving problems of ideal hydrodynamics and magnetohydrodynamics related to the stability of rotating flows of an incompressible fluid (Eckhoff 1981; Lifshitz 1987; Lifschitz 1991; Lifschitz & Hameiri 1991, 1993; Friedlander & Vishik 1995; Lifschitz *et al.* 1996; Kucherenko & Kryvko 2013). It was extended to the viscous and resistive cases in Lifschitz (1991), Dobrokhotov & Shafarevich (1992), Eckhardt & Yao (1995), Kirillov (2013), Kirillov *et al.* (2014), Allilueva & Shafarevich (2015). In particular, this technique allowed one to find analytically neutral stability surfaces in the parameter space, the frequencies of the unstable modes and their growth rates, that agreed well with the numerical simulations (Eckhardt & Yao 1995; Lifschitz *et al.* 1996; Kirillov *et al.* 2014; Child *et al.* 2015; Stefani & Kirillov 2015).

In this paper we apply the geometric optics stability analysis to circular Couette flow of a viscous Newtonian fluid with a temperature gradient in the absence of gravity, but retaining the term of the centrifugal buoyancy. We derive a system of

characteristic equations that includes the transport equations for the lowest-order amplitude of the envelope of the localized perturbation and find a dispersion relation that takes into account the radial variation of the angular velocity and the temperature as well as the kinematic viscosity and the thermal diffusivity.

Using algebraic stability criteria for localization of the roots of polynomials in the left half of the complex plane, we obtain two stability conditions in compact and explicit form; one of them generalizes the Rayleigh discriminant for stationary axisymmetric instabilities to include viscosity effects, and the other provides a marginal stability curve in the parameter plane for oscillatory instabilities. Codimension-2 points on the marginal stability thresholds are identified and the growth rates and frequencies of the instabilities are found analytically. The theoretical results are applied to cylindrical Couette flow with the parameters evaluated at the geometric mean radius both in the Rayleigh unstable and in the Rayleigh stable regimes. In the case of a sole inner cylinder rotating we confirm and extend the numerical results of Meyer *et al.* (2015) and provide analytical expressions for the onset of oscillatory and stationary instabilities, the coordinates of the codimension-2 points, and the Hopf frequency. In the case of a sole outer cylinder rotation, solid body rotation, and rotating flow with Keplerian shear we find a destabilizing effect of the inward temperature gradient that leads to oscillatory instability at small values of the Prandtl number ($Pr < 1$) and to stationary instability at $Pr > 1$.

2. Equations of motion

We consider the flow of an incompressible viscous fluid of density ρ, kinematic viscosity ν and thermal diffusivity κ in the presence of a radial temperature gradient applied to a differentially rotating cylindrical annulus. The ratio $Pr = \nu/\kappa$ constitutes the Prandtl number.

The governing equations written in the inertial frame of reference read (Yoshikawa *et al.* 2013; Meyer *et al.* 2015):

$$\boldsymbol{\nabla}\cdot\boldsymbol{u} = 0, \tag{2.1}$$

$$\frac{\partial \boldsymbol{u}}{\partial t} + \boldsymbol{u}\cdot\boldsymbol{\nabla}\boldsymbol{u} + \frac{1}{\rho}\boldsymbol{\nabla}p - \nu\Delta\boldsymbol{u} + \alpha\theta\boldsymbol{g}_c = 0, \tag{2.2}$$

$$\frac{\partial \theta}{\partial t} + \boldsymbol{u}\cdot\boldsymbol{\nabla}\theta - \kappa\Delta\theta = 0, \tag{2.3}$$

where p is the pressure and θ is the temperature deviation from a reference temperature. The parameter α is the coefficient of thermal expansion.

The flow equations are written in cylindrical coordinates (r, φ, z) in which the velocity field $\boldsymbol{u} = (u, v, w)^{\mathrm{T}}$, where the superscript T denotes transposition. The term $\boldsymbol{u}\cdot\boldsymbol{\nabla}\boldsymbol{u}$ contains the centrifugal-like acceleration $\boldsymbol{g}_c = (v^2/r, 0, 0)^{\mathrm{T}}$ and the Coriolis-like acceleration $(0, uv/r, 0)^{\mathrm{T}}$ coming from the geometry. The Oberbeck–Boussinesq approximation (Chandrasekhar 1961) is used, i.e. we assume small variations of the density with temperature only in the centrifugal force term leading to the centrifugal buoyancy while the other fluid properties (ν, κ, α) are kept constant. This approximation allows one to keep the flow incompressibility condition and eliminates the acoustic modes from the problem analysis. The application of the Oberbeck–Boussinesq approximation to rotating flows can be found in Lopez, Marques & Avila (2013). The gravity g is neglected in order to focus only on the destabilization effects of the centrifugal buoyancy $\alpha\theta\boldsymbol{g}_c$.

We assume that the cylindrical annulus has an infinite length. The system (2.1)–(2.3) possesses a stationary axisymmetric solution describing the base flow state: $\boldsymbol{u}_B = (0, V(r) = r\Omega(r), 0)^{\mathrm{T}}$, $p_B = P(r)$, and $\theta_B = \Theta(r)$. Consider a perturbation of this base flow state: $\boldsymbol{u} = \boldsymbol{u}_B + \widetilde{\boldsymbol{u}}$, $p = p_B + \widetilde{p}$, and $\theta = \theta_B + \widetilde{\theta}$. Then the equations of the flow perturbations linearized around the base flow state read

$$\nabla \cdot \widetilde{\boldsymbol{u}} = 0, \tag{2.4}$$

$$\frac{\partial \widetilde{\boldsymbol{u}}}{\partial t} + \boldsymbol{u}_B \cdot \nabla \widetilde{\boldsymbol{u}} + \widetilde{\boldsymbol{u}} \cdot \nabla \boldsymbol{u}_B - \nu \Delta \widetilde{\boldsymbol{u}} + \frac{1}{\rho} \nabla \widetilde{p} + \alpha \theta_B \widetilde{\boldsymbol{g}}_c + \alpha \widetilde{\theta} \boldsymbol{g}_{cB} = 0, \tag{2.5}$$

$$\frac{\partial \widetilde{\theta}}{\partial t} + \boldsymbol{u}_B \cdot \nabla \widetilde{\theta} + \widetilde{\boldsymbol{u}} \cdot \nabla \theta_B - \kappa \Delta \widetilde{\theta} = 0, \tag{2.6}$$

with the basic centrifugal gravity $\boldsymbol{g}_{cB} = (r\Omega^2, 0, 0)^{\mathrm{T}}$ and the perturbative centrifugal gravity $\widetilde{\boldsymbol{g}}_c = (2\Omega\widetilde{v}, 0, 0)^{\mathrm{T}}$ so that we can write the centrifugal buoyancy terms as follows

$$\alpha \theta_B \widetilde{\boldsymbol{g}}_c = 2\Omega \alpha \theta_B \boldsymbol{e}_r \boldsymbol{e}_\varphi^{\mathrm{T}} \widetilde{\boldsymbol{u}}, \tag{2.7}$$

$$\alpha \widetilde{\theta} \boldsymbol{g}_{cB} = \alpha \widetilde{\theta} r \Omega^2 \boldsymbol{e}_r, \tag{2.8}$$

where $\boldsymbol{e}_r$ and $\boldsymbol{e}_\varphi$ are radial and azimuthal unit vectors, respectively.

The gradients of the background fields are

$$\nabla \boldsymbol{u}_B = \Omega \begin{pmatrix} 0 & -1 & 0 \\ 1 + 2Ro & 0 & 0 \\ 0 & 0 & 0 \end{pmatrix}, \quad \nabla \theta_B = \begin{pmatrix} D\Theta \\ 0 \\ 0 \end{pmatrix}, \tag{2.9a,b}$$

where

$$Ro = \frac{rD\Omega}{2\Omega} \tag{2.10}$$

is the Rossby number and $D = \mathrm{d}/\mathrm{d}r$. Denoting $\mathcal{U} = \nabla \boldsymbol{u}_B$, we formulate the linearized equations of motion in the final form:

$$\nabla \cdot \widetilde{\boldsymbol{u}} = 0, \tag{2.11}$$

$$\left(\frac{\partial}{\partial t} + \mathcal{U} + 2\Omega \alpha \theta_B \boldsymbol{e}_r \boldsymbol{e}_\varphi^{\mathrm{T}} + \boldsymbol{u}_B \cdot \nabla \right) \widetilde{\boldsymbol{u}} - \nu \Delta \widetilde{\boldsymbol{u}} + \frac{1}{\rho} \nabla \widetilde{p} + \alpha r \Omega^2 \boldsymbol{e}_r \widetilde{\theta} = 0, \tag{2.12}$$

$$\left(\frac{\partial}{\partial t} + \boldsymbol{u}_B \cdot \nabla \right) \widetilde{\theta} + \widetilde{\boldsymbol{u}} \cdot \nabla \theta_B - \kappa \Delta \widetilde{\theta} = 0. \tag{2.13}$$

3. Evolution of the localized perturbations

Let ϵ be a small parameter ($0 < \epsilon \ll 1$). We are looking for a solution of the linearized equations (2.11)–(2.13) in the form of the generalized progressive wave expansions (Eckhoff 1981)

$$\widetilde{\boldsymbol{u}} = \left(\boldsymbol{u}^{(0)}(\boldsymbol{x}, t) + \epsilon \boldsymbol{u}^{(1)}(\boldsymbol{x}, t) \right) \exp\left(\mathrm{i}\epsilon^{-1} \Phi(\boldsymbol{x}, t) \right) + \epsilon \boldsymbol{u}^{(r)}(\boldsymbol{x}, t, \epsilon), \tag{3.1}$$

$$\widetilde{\theta} = \left(\theta^{(0)}(\boldsymbol{x}, t) + \epsilon \theta^{(1)}(\boldsymbol{x}, t) \right) \exp\left(\mathrm{i}\epsilon^{-1} \Phi(\boldsymbol{x}, t) \right) + \epsilon \theta^{(r)}(\boldsymbol{x}, t, \epsilon), \tag{3.2}$$

$$\widetilde{p} = \left(p^{(0)}(\boldsymbol{x}, t) + \epsilon p^{(1)}(\boldsymbol{x}, t) \right) \exp\left(\mathrm{i}\epsilon^{-1} \Phi(\boldsymbol{x}, t) \right) + \epsilon p^{(r)}(\boldsymbol{x}, t, \epsilon), \tag{3.3}$$

where Φ is generally a complex-valued scalar function that represents the phase of the wave or the eikonal and the remainder terms $\boldsymbol{u}^{(r)}, \theta^{(r)}, p^{(r)}$ are assumed to be uniformly bounded in ϵ on any fixed time interval (Eckhoff 1981; Lifschitz 1991; Lifschitz & Hameiri 1991, 1993; Lifschitz *et al.* 1996).

Maslov (1986) observed that high-frequency oscillations $\exp(\mathrm{i}\epsilon^{-1}\Phi(\boldsymbol{x}, t))$ quickly die out because of viscosity unless one assumes a quadratic dependency of viscosity on the small parameter ϵ. Hence, following (Maslov 1986; Dobrokhotov & Shafarevich 1992; Kirillov *et al.* 2014; Allilueva & Shafarevich 2015), we assume that $\nu = \epsilon^2\widetilde{\nu}$ and $\kappa = \epsilon^2\widetilde{\kappa}$.

Substituting the asymptotic series (3.1) into the incompressibility condition (2.11) and collecting terms at ϵ^{-1} and ϵ^0, we find

$$\epsilon^{-1}: \quad \boldsymbol{u}^{(0)} \cdot \nabla\Phi = 0, \tag{3.4}$$

$$\epsilon^{0}: \quad \nabla \cdot \boldsymbol{u}^{(0)} + \mathrm{i}\boldsymbol{u}^{(1)} \cdot \nabla\Phi = 0. \tag{3.5}$$

A similar procedure applied to (2.12) and (2.13) yields the two systems of equations

$$\epsilon^{-1}: \quad \begin{pmatrix} \dfrac{\partial\Phi}{\partial t} + \boldsymbol{u}_B \cdot \nabla\Phi & 0 \\ 0 & \dfrac{\partial\Phi}{\partial t} + \boldsymbol{u}_B \cdot \nabla\Phi \end{pmatrix} \begin{pmatrix} \boldsymbol{u}^{(0)} \\ \theta^{(0)} \end{pmatrix} = -\frac{\nabla\Phi}{\rho} \begin{pmatrix} p^{(0)} \\ 0 \end{pmatrix}, \tag{3.6}$$

$$\begin{aligned} \epsilon^{0}: \quad & \mathrm{i} \begin{pmatrix} \dfrac{\partial\Phi}{\partial t} + \boldsymbol{u}_B \cdot \nabla\Phi & 0 \\ 0 & \dfrac{\partial\Phi}{\partial t} + \boldsymbol{u}_B \cdot \nabla\Phi \end{pmatrix} \begin{pmatrix} \boldsymbol{u}^{(1)} \\ \theta^{(1)} \end{pmatrix} = -\mathrm{i}\frac{\nabla\Phi}{\rho} \begin{pmatrix} p^{(1)} \\ 0 \end{pmatrix} \\ & - \begin{pmatrix} \dfrac{\partial}{\partial t} + \boldsymbol{u}_B \cdot \nabla + \mathcal{U} + \widetilde{\nu}(\nabla\Phi)^2 & 0 \\ 0 & \dfrac{\partial}{\partial t} + \boldsymbol{u}_B \cdot \nabla + \widetilde{\kappa}(\nabla\Phi)^2 \end{pmatrix} \begin{pmatrix} \boldsymbol{u}^{(0)} \\ \theta^{(0)} \end{pmatrix} \\ & - \begin{pmatrix} 2\Omega\alpha\theta_B \boldsymbol{e}_r \boldsymbol{e}_\varphi^{\mathrm{T}} & \alpha r\Omega^2 \boldsymbol{e}_r \\ (\nabla\theta_B)^{\mathrm{T}} & 0 \end{pmatrix} \begin{pmatrix} \boldsymbol{u}^{(0)} \\ \theta^{(0)} \end{pmatrix} - \frac{\nabla}{\rho} \begin{pmatrix} p^{(0)} \\ 0 \end{pmatrix}. \end{aligned} \tag{3.7}$$

The amplitudes with the superscript (0) are contained both in (3.6) corresponding to the lowest degree of ϵ equal to -1 and in (3.7) corresponding to the degree 0. Therefore, finding the lowest-order amplitudes with the superscript (0) requires an iterative procedure involving both (3.6) and (3.7).

Taking the dot product of the first of the equations in the system (3.6) with $\nabla\Phi$ under the constraint (3.4) we find that for $\nabla\Phi \neq 0$

$$p^{(0)} = 0. \tag{3.8}$$

Under the condition (3.8) the system (3.6) has a non-trivial solution if the determinant of the 4×4 matrix in its left-hand side is vanishing. This gives us a 4-fold characteristic root corresponding to the Hamilton–Jacobi equation

$$\frac{\partial\Phi}{\partial t} + \boldsymbol{u}_B \cdot \nabla\Phi = 0, \tag{3.9}$$

with the initial data: $\Phi(\boldsymbol{x}, 0) = \Phi_0(\boldsymbol{x})$.

Taking the gradient of (3.9) yields the eikonal equation (Lifschitz & Hameiri 1991)

$$\left(\frac{\partial}{\partial t}+\boldsymbol{u}_B\cdot\boldsymbol{\nabla}\right)\boldsymbol{\nabla}\Phi+\boldsymbol{\nabla}\boldsymbol{u}_B\cdot\boldsymbol{\nabla}\Phi=0, \tag{3.10}$$

with the initial condition $\boldsymbol{\nabla}\Phi(\boldsymbol{x},0)=\boldsymbol{\nabla}\Phi_0(\boldsymbol{x})$. In the notation $\boldsymbol{k}=\boldsymbol{\nabla}\Phi$ and $(\mathrm{d}/\mathrm{d}t)=(\partial/\partial t)+\boldsymbol{u}_B\cdot\boldsymbol{\nabla}$ the eikonal equation (3.10) is (Lifschitz 1991)

$$\frac{\mathrm{d}\boldsymbol{k}}{\mathrm{d}t}=-\boldsymbol{\nabla}\boldsymbol{u}_B\cdot\boldsymbol{k}=-\mathcal{U}^{\mathrm{T}}\boldsymbol{k}, \tag{3.11}$$

where $\mathcal{U}^{\mathrm{T}}$ denotes the transposed 3×3 matrix $\mathcal{U}$ (Eckhardt & Yao 1995).

Relations (3.8) and (3.9) allow us to reduce the system (3.7) to

$$\left(\frac{\mathrm{d}}{\mathrm{d}t}+\mathcal{U}+\widetilde{\nu}(\boldsymbol{\nabla}\Phi)^2+2\alpha\Omega\theta_B\boldsymbol{e}_r\boldsymbol{e}_\varphi^{\mathrm{T}}\right)\boldsymbol{u}^{(0)}+\alpha r\Omega^2\boldsymbol{e}_r\theta^{(0)}=-\frac{\mathrm{i}\boldsymbol{\nabla}\Phi}{\rho}p^{(1)}, \tag{3.12}$$

$$(\boldsymbol{\nabla}\theta_B)^{\mathrm{T}}\boldsymbol{u}^{(0)}+\left(\frac{\mathrm{d}}{\mathrm{d}t}+\widetilde{\kappa}(\boldsymbol{\nabla}\Phi)^2\right)\theta^{(0)}=0. \tag{3.13}$$

Multiplying (3.12) with $\boldsymbol{\nabla}\Phi$ from the left, we isolate the pressure term

$$p^{(1)}=\mathrm{i}\rho\frac{\boldsymbol{\nabla}\Phi}{(\boldsymbol{\nabla}\Phi)^2}\cdot\left(\left[\frac{\mathrm{d}}{\mathrm{d}t}+\mathcal{U}+2\alpha\Omega\theta_B\boldsymbol{e}_r\boldsymbol{e}_\varphi^{\mathrm{T}}\right]\boldsymbol{u}^{(0)}+\alpha r\Omega^2\boldsymbol{e}_r\theta^{(0)}\right). \tag{3.14}$$

Taking into account the identity (Lifschitz & Hameiri 1991; Kirillov *et al.* 2014)

$$\frac{\mathrm{d}}{\mathrm{d}t}(\boldsymbol{\nabla}\Phi\cdot\boldsymbol{u}^{(0)})=\frac{\mathrm{d}\boldsymbol{\nabla}\Phi}{\mathrm{d}t}\cdot\boldsymbol{u}^{(0)}+\boldsymbol{\nabla}\Phi\cdot\frac{\mathrm{d}\boldsymbol{u}^{(0)}}{\mathrm{d}t}=0 \tag{3.15}$$

we modify (3.14) in the following way

$$p^{(1)}=\mathrm{i}\rho\frac{\boldsymbol{\nabla}\Phi}{(\boldsymbol{\nabla}\Phi)^2}\cdot\left((\mathcal{U}+2\alpha\Omega\theta_B\boldsymbol{e}_r\boldsymbol{e}_\varphi^{\mathrm{T}})\boldsymbol{u}^{(0)}+\alpha r\Omega^2\boldsymbol{e}_r\theta^{(0)}\right)-\mathrm{i}\rho\frac{1}{(\boldsymbol{\nabla}\Phi)^2}\frac{\mathrm{d}\boldsymbol{\nabla}\Phi}{\mathrm{d}t}\cdot\boldsymbol{u}^{(0)}. \tag{3.16}$$

Now using (3.11) we re-write (3.16) in terms of the wave vector $\boldsymbol{k}$

$$p^{(1)}=2\mathrm{i}\rho\alpha\Omega\theta_B\frac{\boldsymbol{k}^{\mathrm{T}}\boldsymbol{e}_r\boldsymbol{e}_\varphi^{\mathrm{T}}}{|\boldsymbol{k}|^2}\boldsymbol{u}^{(0)}+\mathrm{i}\rho\alpha r\Omega^2\frac{\boldsymbol{k}^{\mathrm{T}}\boldsymbol{e}_r}{|\boldsymbol{k}|^2}\theta^{(0)}+2\mathrm{i}\rho\frac{\boldsymbol{k}^{\mathrm{T}}\mathcal{U}}{|\boldsymbol{k}|^2}\boldsymbol{u}^{(0)}. \tag{3.17}$$

Substituting (3.17) into (3.12) we finally arrive at the transport equations for the leading-order amplitudes $\boldsymbol{u}^{(0)}$ and $\theta^{(0)}$ in the expansions (3.1) and (3.2):

$$\begin{aligned}\frac{\mathrm{d}\boldsymbol{u}^{(0)}}{\mathrm{d}t}&=-\widetilde{\nu}|\boldsymbol{k}|^2\boldsymbol{u}^{(0)}-\left(\mathcal{I}-2\frac{\boldsymbol{k}\boldsymbol{k}^{\mathrm{T}}}{|\boldsymbol{k}|^2}\right)\mathcal{U}\boldsymbol{u}^{(0)}-2\alpha\Omega\theta_B\left(\mathcal{I}-\frac{\boldsymbol{k}\boldsymbol{k}^{\mathrm{T}}}{|\boldsymbol{k}|^2}\right)\boldsymbol{e}_r\boldsymbol{e}_\varphi^{\mathrm{T}}\boldsymbol{u}^{(0)}\\&\quad-\alpha r\Omega^2\left(\mathcal{I}-\frac{\boldsymbol{k}\boldsymbol{k}^{\mathrm{T}}}{|\boldsymbol{k}|^2}\right)\boldsymbol{e}_r\theta^{(0)},\end{aligned} \tag{3.18}$$

$$\frac{\mathrm{d}\theta^{(0)}}{\mathrm{d}t}=-\widetilde{\kappa}|\boldsymbol{k}|^2\theta^{(0)}-(\boldsymbol{\nabla}\theta_B)^{\mathrm{T}}\boldsymbol{u}^{(0)}, \tag{3.19}$$

with $\mathcal{I}$ the 3×3 identity matrix and the initial data $\boldsymbol{u}^{(0)}(\boldsymbol{x},0)=\boldsymbol{u}_0^{(0)}(\boldsymbol{x})$ and $\theta^{(0)}(\boldsymbol{x},0)=\theta_0^{(0)}(\boldsymbol{x})$.

Note that the leading-order terms dominate the solution (3.1) and (3.2) for a sufficiently long time, provided that ϵ is small enough (Lifschitz 1991; Lifschitz *et al.* 1996), which reduces analysis of instabilities to the investigation of the growth rates of solutions of the transport equations (3.18) and (3.19).

Let us consider a fluid element with the trajectory passing through a point $\boldsymbol{x}_0$ at the initial moment $t=0$:

$$\frac{\mathrm{d}\boldsymbol{x}}{\mathrm{d}t}=\boldsymbol{u}_B, \quad \boldsymbol{x}(0)=\boldsymbol{x}_0. \tag{3.20a,b}$$

Then, the eikonal equation (3.11) can be interpreted as an ordinary differential equation describing the evolution of the wave vector $\boldsymbol{k}(t)=\nabla\Phi(\boldsymbol{x}(t),\,t)$ along the stream line (3.20) with the initial condition $\boldsymbol{k}(0)=\boldsymbol{k}_0=\nabla\Phi_0(\boldsymbol{x}_0)$. Consequently, the transport equations (3.18) and (3.19) can also be treated as a system of ODEs along the stream lines of the flow for the amplitudes $\boldsymbol{u}^{(0)}(\boldsymbol{x}(t),\,t)$ and $\theta^{(0)}(\boldsymbol{x}(t),\,t)$ with the initial data $\boldsymbol{u}^{(0)}(0)=\boldsymbol{u}_0^{(0)}(\boldsymbol{x}_0)$ and $\theta^{(0)}(0)=\theta_0^{(0)}(\boldsymbol{x}_0)$. Therefore, the characteristic equations (3.20), (3.11), (3.18) and (3.19) describe motion of the envelope of a perturbation localized at the initial moment of time at $\boldsymbol{x}_0$ along with the particles in the fluid flow that pass through $\boldsymbol{x}_0$ at $t=0$.

4. Dispersion relation and its parameterizations

Following the procedure described in Friedlander & Vishik (1995) we write the eikonal equation (3.11) in cylindrical coordinates $r,\,\varphi,\,z$

$$\frac{\partial\boldsymbol{k}}{\partial t}=\begin{pmatrix}0 & -2\Omega Ro & 0\\ 0 & 0 & 0\\ 0 & 0 & 0\end{pmatrix}\boldsymbol{k}(t) \tag{4.1}$$

and consider the bounded, and asymptotically non-decaying and non-diverging solution of (4.1) with $k_r=\text{const.}$, $k_\varphi=0$, and $k_z=\text{const.}$ (Eckhardt & Yao 1995; Friedlander & Vishik 1995). With this, we can write the amplitude transport equations (3.18) in coordinate form as

$$\left[\frac{\partial}{\partial t}+\Omega\frac{\partial}{\partial\varphi}+\widetilde{\nu}|\boldsymbol{k}|^2\right]u_r^{(0)}=\beta^2\left[2\Omega(1-\alpha\theta_B)u_\varphi^{(0)}-\alpha r\Omega^2\theta^{(0)}\right], \tag{4.2}$$

$$\left[\frac{\partial}{\partial t}+\Omega\frac{\partial}{\partial\varphi}+\widetilde{\nu}|\boldsymbol{k}|^2\right]u_\varphi^{(0)}=-2\Omega(1+Ro)u_r^{(0)}, \tag{4.3}$$

$$\left[\frac{\partial}{\partial t}+\Omega\frac{\partial}{\partial\varphi}+\widetilde{\kappa}|\boldsymbol{k}|^2\right]\theta^{(0)}=-D\Theta u_r^{(0)}, \tag{4.4}$$

$$\left[\frac{\partial}{\partial t}+\Omega\frac{\partial}{\partial\varphi}+\widetilde{\nu}|\boldsymbol{k}|^2\right]u_z^{(0)}=-\beta^2\frac{k_r}{k_z}\left[2\Omega(1-\alpha\theta_B)u_\varphi^{(0)}-\alpha r\Omega^2\theta^{(0)}\right], \tag{4.5}$$

where $\beta=k_z|\boldsymbol{k}|^{-1}$ and $|\boldsymbol{k}|=\sqrt{k_r^2+k_z^2}$.

We see that (4.2)–(4.4) form a closed sub-system with respect to $u_r^{(0)}$, $u_\varphi^{(0)}$ and $\theta^{(0)}$. Indeed, the transformation $u_z^{(0)}\to(-k_r/k_z)u_r^{(0)}$ makes (4.5) equivalent to (4.2). Following (Friedlander & Vishik 1995) we will look for a solution to this sub-system in the modal form as $\theta^{(0)}=\hat{\theta}\mathrm{e}^{\lambda t+\mathrm{i}m\varphi}$, and write the amplitude equations in the matrix

form $\boldsymbol{H}\xi = \lambda\xi$, where $\xi = (\hat{u}_r, \hat{u}_\varphi, \hat{\theta})^{\mathrm{T}}$ is the eigenvector associated with the eigenvalue λ of the matrix (cf. (A 19) that is obtained in the narrow-gap approximation)

$$\boldsymbol{H} = \begin{pmatrix} -\mathrm{i}m\Omega - \widetilde{\nu}|\boldsymbol{k}|^2 & 2\Omega\beta^2(1-\alpha\Theta) & -\alpha r\Omega^2\beta^2 \\ -2\Omega(1+Ro) & -\mathrm{i}m\Omega - \widetilde{\nu}|\boldsymbol{k}|^2 & 0 \\ -D\Theta & 0 & -\mathrm{i}m\Omega - \widetilde{\kappa}|\boldsymbol{k}|^2 \end{pmatrix}. \tag{4.6}$$

The solvability condition for a non-trivial solution yields the dispersion relation

$$p(\lambda) = \det(\boldsymbol{H} - \lambda\boldsymbol{I}) = 0, \tag{4.7}$$

where $\boldsymbol{I}$ is the 3×3-unit matrix. (Note that a similar dispersion relation was derived also in Economides & Moir (1980) in the case when the radial acceleration $\boldsymbol{g}$ does not depend on r (see appendix A). In our case $\boldsymbol{g}(r) = \boldsymbol{g}_{cB} = (r\Omega^2, 0, 0)^{\mathrm{T}}$.)

Let us introduce the non-dimensional parameters

$$Ta = \frac{\beta\Omega}{\widetilde{\nu}|\boldsymbol{k}|^2}, \quad \hat{\Theta} = \frac{\Theta}{\Delta T}, \quad \gamma_a = \alpha\Delta T, \quad Rt = \frac{rD\Theta}{2\Theta}, \quad n = \frac{m}{\beta}, \quad s = \frac{\lambda}{\beta\Omega}, \tag{4.8a–f}$$

where Ta is the Taylor number, Rt is the thermal analogue of the Rossby number and measures the local slope of the temperature profile (not to be confused with the thermal Rossby number used in atmospheric physics (Lappa 2012)), ΔT is the temperature difference imposed at the cylindrical surfaces bounding the flow, $\hat{\Theta}$ represents the dimensionless temperature, n is a modified azimuthal wavenumber, and s is a dimensionless eigenvalue. Introducing the diagonal matrix $\boldsymbol{R} = \mathrm{diag}(1, 1, \Delta T/r)$, we transform (4.6) into

$$\boldsymbol{R}^{-1}\boldsymbol{H}\boldsymbol{R} = \beta\Omega \begin{pmatrix} -\mathrm{i}n - \dfrac{1}{Ta} & 2\beta(1-\gamma_a\hat{\Theta}) & -\gamma_a\beta\Omega \\ -\dfrac{2}{\beta}(1+Ro) & -\mathrm{i}n - \dfrac{1}{Ta} & 0 \\ -2\hat{\Theta}Rt\dfrac{1}{\beta\Omega} & 0 & -\mathrm{i}n - \dfrac{1}{TaPr} \end{pmatrix} \tag{4.9}$$

and re-write the dispersion relation (4.7) in the equivalent form

$$\det(\boldsymbol{R}^{-1}\boldsymbol{H}\boldsymbol{R} - s\beta\Omega\boldsymbol{I}) = -\beta^3\Omega^3 q(s) = 0, \tag{4.10}$$

where $q(s)$ is a third-degree polynomial with complex coefficients that does not contain the parameters β and Ω and depends entirely on the dimensionless control parameters Ta, Pr, $\hat{\Theta}$, γ_a, n and on the logarithmic derivatives of the velocity and temperature profiles of the base flow represented by the dimensionless hydrodynamic and thermal Rossby numbers Ro and Rt, respectively.

Introducing the new spectral variable $\chi = s + \mathrm{i}n$ into the complex dispersion relation $q(s) = 0$, we transform it into a real third-degree polynomial equation in χ:

$$\chi^3 + a_2\chi^2 + a_1\chi + a_0 = 0. \tag{4.11}$$

The real coefficients a_i of the characteristic polynomial (4.11) depend on the dimensionless flow parameters as follows:

$$a_0 = \frac{1}{Ta}\left[\frac{1}{PrTa^2} + \frac{4(1+Ro)(1-\gamma_a\hat{\Theta})}{Pr} - 2\gamma_a\hat{\Theta}Rt\right], \tag{4.12}$$

Rotation case	Ro	Pr^S	Pr^H
Inner cylinder	$-\dfrac{1}{1-\eta}$	$-\dfrac{4\eta\ln\eta}{1-\eta}\left(\dfrac{1}{\gamma_a}-\dfrac{1}{2}\right)$	$-\left[1+\dfrac{8\eta\ln\eta}{1-\eta}\left(\dfrac{1}{\gamma_a}-\dfrac{1}{2}\right)\right]^{-1}$
Outer cylinder	$\dfrac{\eta}{1-\eta}$	$\dfrac{4\ln\eta}{1-\eta}\left(\dfrac{1}{\gamma_a}-\dfrac{1}{2}\right)$	$-\left[1-\dfrac{8\ln\eta}{1-\eta}\left(\dfrac{1}{\gamma_a}-\dfrac{1}{2}\right)\right]^{-1}$
Keplerian	$-\dfrac{1+\sqrt{\eta}+\eta}{(1+\sqrt{\eta})^2}$	$\dfrac{4\sqrt{\eta}\ln\eta}{(1+\sqrt{\eta})^2}\left(\dfrac{1}{\gamma_a}-\dfrac{1}{2}\right)$	$-\left[1-\dfrac{8\sqrt{\eta}\ln\eta}{(1+\sqrt{\eta})^2}\left(\dfrac{1}{\gamma_a}-\dfrac{1}{2}\right)\right]^{-1}$
Solid body	0	$4\ln\eta\left(\dfrac{1}{\gamma_a}-\dfrac{1}{2}\right)$	$-\left[1-8\ln\eta\left(\dfrac{1}{\gamma_a}-\dfrac{1}{2}\right)\right]^{-1}$

TABLE 1. Rossby numbers for different rotating cases of the Couette–Taylor system according to (4.16) and the corresponding asymptotic values (6.4) and (6.10) that bound the intervals of Pr at which stationary (Pr^S) and oscillatory (Pr^H) modes are admissible.

$$a_1 = 4(1+Ro)(1-\gamma_a\hat{\Theta}) - 2\gamma_a\hat{\Theta}Rt + \frac{Pr+2}{PrTa^2}, \tag{4.13}$$

$$a_2 = \frac{2Pr+1}{TaPr}. \tag{4.14}$$

The set of dimensionless parameters (4.8) is convenient for applications in astrophysical gasdynamics (Acheson & Gibbons 1978; Balbus & Potter 2016). In order to facilitate comparison with the experimental data we need to express these parameters in terms of the realistic Taylor–Couette system. In this case, the base flow state confined in the gap between two coaxial cylinders of radii a and b rotating with the angular frequencies Ω_a and Ω_b, respectively, is given by (Chandrasekhar 1961; Ali & Weidman 1990; Meyer *et al.* 2015)

$$\Omega = \frac{\mu-\eta^2}{1-\eta^2} + \frac{1-\mu}{1-\eta^2}\frac{\eta^2}{(1-\eta)^2}\frac{1}{r^2}, \quad \hat{\Theta} = \frac{\ln(1-\eta)r}{\ln\eta}, \tag{4.15a,b}$$

where $\eta = a/b < 1$ is the radius ratio and $\mu = \Omega_b/\Omega_a$ is the rotation ratio. The angular velocity is measured in units of Ω_a and the radial distance in units of $d = b - a$.

Evaluating the parameters (2.10), (4.8) and (4.15) at the geometric mean radius $r_g = \sqrt{\eta}/(1-\eta)$ (as proposed by Dubrulle *et al.* (2005)), we find (in the case of counter-rotating cylinders, the hydrodynamic Rossby number diverges at $\mu = -\eta$; for $\mu \leqslant -\eta$, one may choose the geometric mean radius of the potentially unstable zone)

$$\hat{\Theta} = \frac{1}{2}, \quad Rt = \frac{1}{\ln\eta}, \quad Ro = -1 + \frac{\mu-\eta^2}{(1-\eta)(\eta+\mu)}. \tag{4.16a–c}$$

Relations (4.16) allow us to interpret the local Rossby numbers Ro and Rt in terms of the radius and velocity ratios η and μ of the realistic Taylor–Couette cell, see table 1 containing the four different rotation cases: sole rotation of the inner cylinder ($\mu = 0$), Keplerian rotation ($\mu = \eta^{3/2}$), sole rotation of the outer cylinder ($\mu \to \infty$), and solid body rotation ($\mu = 1$). In particular, $Rt < 0$ for the Taylor–Couette system due to the geometric constraint $0 < \eta < 1$ and the temperature variation is such that $0 \leqslant \hat{\Theta} \leqslant 1$.

5. Local instabilities

5.1. *Diffusionless instabilities*

In the case when the viscosity and thermal diffusivity are both set to zero in (4.6) or, equivalently, $Ta \to \infty$ in (4.9), the dispersion relation (4.11) factorizes to

$$\chi(\chi^2 + 4(1+Ro)(1-\gamma_a\hat{\Theta}) - 2\gamma_a\hat{\Theta}Rt) = 0. \tag{5.1}$$

The root $\chi = 0$ corresponds to the pure imaginary eigenvalue $\lambda = \beta\Omega s = -\mathrm{i}m\Omega$ describing a stable rotating wave with the local frequency Ω. Similarly, the flow admits stable inertial waves with frequencies given by

$$\frac{\omega}{\Omega} = -m \pm \beta\sqrt{4(1+Ro)(1-\gamma_a\hat{\Theta}) - 2\gamma_a\hat{\Theta}Rt}, \tag{5.2}$$

if the radicand in (5.2) is positive:

$$4(1+Ro)(1-\gamma_a\hat{\Theta}) - 2\gamma_a\hat{\Theta}Rt > 0. \tag{5.3}$$

These inertial waves result from the combined effects of the rotation and the temperature gradient. While the term $\gamma_a\hat{\Theta}$ is very weak in the Boussinesq approximation, the term $\gamma_a\hat{\Theta}Rt$ can become significant depending on the steepness of the temperature profile. In the isothermal case ($\gamma_a = 0$), we retrieve the frequency of the Kelvin waves in rotating flows.

The inequality (5.3) contains the generalized Rayleigh criterion derived in Mutabazi & Bahloul (2002) and Meyer *et al.* (2015) for the stability of inviscid flow with curved streamlines and a radial temperature gradient. Indeed, Mutabazi & Bahloul (2002) and Meyer *et al.* (2015) found the criterion for stability against axisymmetric perturbations in the diffusionless case in terms of the generalized Rayleigh discriminant $\Psi(r)$:

$$\Psi(r) > 0, \quad \Psi(r) = \Phi - \gamma_a\left(\hat{\Theta}\Phi + \frac{\mathrm{d}\hat{\Theta}}{\mathrm{d}r}\frac{V^2}{r}\right), \quad \Phi(r) = \frac{1}{r^3}\frac{\mathrm{d}(rV)^2}{\mathrm{d}r}. \tag{5.4a–c}$$

Expressing the classical hydrodynamic Rayleigh discriminant $\Phi(r)$ via the hydrodynamic Rossby number as $\Phi = 4\Omega^2(1+Ro)$, we obtain

$$\Psi = \Omega^2\{4(1+Ro) - 2\gamma_a\hat{\Theta}[Rt + 2(1+Ro)]\}. \tag{5.5}$$

Requiring $\Psi > 0$ we arrive exactly at the criterion (5.3). The opposite inequality $\Psi < 0$ or $4(1+Ro)(1-\gamma_a\hat{\Theta}) - 2\gamma_a\hat{\Theta}Rt < 0$ coincides with the condition for instability to stationary axisymmetric perturbations known as the diffusionless Goldreich–Schubert–Fricke (GSF) instability (Acheson & Gibbons 1978).

5.2. *Enhancement of stability by viscosity and thermal diffusivity at $Pr = 1$*

In the case when $Pr = 1$ (i.e. when the viscous and thermal diffusion timescales are equal) the dispersion relation (4.11) can also be factorized:

$$\left(\chi + \frac{1}{Ta}\right)\left[\left(\chi + \frac{1}{Ta}\right)^2 + 4(1-\gamma_a\hat{\Theta})(1+Ro) - 2\gamma_a\hat{\Theta}Rt\right] = 0. \tag{5.6}$$

By this reasoning, the roots of the dispersion relation (5.6) can be found explicitly:

$$s_{1,2} = -\frac{1}{Ta} - in \pm i\sqrt{4(1+Ro)(1-\gamma_a\hat{\Theta}) - 2\gamma_a\hat{\Theta}Rt}, \tag{5.7}$$

$$s_3 = -\frac{1}{Ta} - in. \tag{5.8}$$

The mode with the eigenvalue s_3 is a pure hydrodynamic mode as it does not contain the temperature gradient, it is damped by the viscosity. The modes corresponding to the eigenvalue $s_{1,2}$ contain both the hydrodynamic and thermal effects. One of the modes is always damped, the other one should be excited when its growth rate vanishes, i.e. when

$$4(1+Ro)(1-\gamma_a\hat{\Theta}) - 2\gamma_a\hat{\Theta}Rt + \frac{1}{Ta^2} = 0. \tag{5.9}$$

The double-diffusive stability criterion given by the requirement for the left-hand side of (5.9) to be positive suggests that at $Pr = 1$ the viscosity and thermal diffusivity enlarge the stability domain of the diffusionless system. Furthermore, in the limit $Ta \to \infty$ the roots (5.7) and (5.8) reduce to the roots of the diffusionless dispersion relation (5.1), whereas the double-diffusive stability criterion reduces to the diffusionless criterion (5.3).

Note that the limiting procedure that first makes the diffusion coefficients of a dissipative system with two diffusion mechanisms equal and then tends them to zero typically yields a correct diffusionless stability criterion in many double-diffusive systems of hydrodynamics and magnetohydrodynamics (Kirillov *et al.* 2014; Kirillov 2016). In general, the limit of zero dissipation of the double-diffusive stability criteria should not necessarily coincide with the diffusionless stability criteria (Acheson & Gibbons 1978; Kirillov & Verhulst 2010; Kirillov 2013).

5.3. *Double-diffusive flow stability criteria at arbitrary Pr*

We derive stability conditions of the base flow at arbitrary Pr by applying the Lienard–Chipart stability criterion (Kirillov 2013) to the real polynomial (4.11) of degree 3 in χ:

$$a_0 > 0, \quad a_2 > 0, \quad -a_0(a_0 - a_1a_2) > 0. \tag{5.10a–c}$$

The second inequality is always fulfilled whereas the first one yields:

$$4(1+Ro)(1-\gamma_a\hat{\Theta}) - 2\gamma_a\hat{\Theta}RtPr + \frac{1}{Ta^2} > 0. \tag{5.11}$$

The condition (5.11) is a modified Rayleigh criterion that takes into account both the kinematic viscosity and the thermal diffusion. Writing it as

$$1 + Ro > \frac{2\gamma_a\hat{\Theta}\,RtPr}{4(1-\gamma_a\hat{\Theta})} - \frac{1}{4Ta^2(1-\gamma_a\hat{\Theta})}, \tag{5.12}$$

we conclude that, for $Rt < 0$ and $0 \leqslant \hat{\Theta} \leqslant 1$, the kinematic viscosity and outward heating ($\gamma_a > 0$) are stabilizing and inward heating ($\gamma_a < 0$) is destabilizing with respect to the Rayleigh criterion ($1 + Ro > 0$) for an ideal incompressible fluid.

At $Pr = 1$ the condition (5.11) reduces to the criterion (5.9). Furthermore, the limit $Ta \to \infty$ applied to (5.11) yields the diffusionless criterion (5.3) only if $Pr = 1$.

The condition $a_0 = 0$ yields the control parameter Ta as a function of the other control parameters:

$$Ta_c^S = \frac{1}{\sqrt{2\gamma_a\hat{\Theta}RtPr - 4(1+Ro)(1-\gamma_a\hat{\Theta})}}. \tag{5.13}$$

Since at $a_0 = 0$ the dispersion equation (4.11) has the root $\chi = 0$, corresponding to $s = -in$, the relation (5.13) is the threshold of the double-diffusive Goldreich–Schubert–Fricke instability (Acheson & Gibbons 1978), which is a stationary axisymmetric instability in the case when $n = 0$.

The third inequality of (5.10) yields

$$-\left(\gamma_a\hat{\Theta}(Pr+1)Rt - 4Pr(1-\gamma_a\hat{\Theta})(1+Ro) - \frac{(Pr+1)^2}{PrTa^2}\right) > 0, \tag{5.14}$$

from which the threshold of the oscillatory instability through a Hopf bifurcation naturally follows:

$$Ta_c^H = \frac{Pr+1}{\sqrt{Pr(Pr+1)\gamma_a\hat{\Theta}Rt - 4Pr^2(1-\gamma_a\hat{\Theta})(1+Ro)}}. \tag{5.15}$$

Indeed, from the Vieta's formulas (Vinberg 2003)

$$\chi_1+\chi_2+\chi_3 = -a_2, \quad \chi_1\chi_2+\chi_2\chi_3+\chi_3\chi_1 = a_1, \quad \chi_1\chi_2\chi_3 = -a_0 \tag{5.16a–c}$$

it follows that at $Ta = Ta_c^H$ the characteristic equation (4.11) admits two imaginary roots $\chi_{1,2} = \pm i\bar{\omega}_c$, corresponding to $s = -in \pm i\bar{\omega}_c$, where n can be either zero or not, and one real root $\chi_3 = -a_2$. The real root corresponds to a damped mode while the imaginary roots yield the Hopf frequency $\bar{\omega}_c$ given by

$$\bar{\omega}_c = \frac{\sqrt{4(1+Ro)(1-\gamma_a\hat{\Theta}) - \gamma_a\hat{\Theta}RtPr(Pr+1)}}{Pr+1} \tag{5.17}$$

and describe a marginal oscillatory mode. The total frequency of this marginal mode is given by $\omega_c = -\beta\Omega(n \pm \bar{\omega}_c)$. The marginal value Ta_c^H corresponds to a Hopf bifurcation of the base flow to a state oscillating with a Hopf frequency $\bar{\omega}_c$. For $n = 0$, the marginal mode is an oscillatory axisymmetric mode, while for $n \neq 0$, the marginal mode is an oscillatory non-axisymmetric mode.

5.4. *Codimension-2 points in the case of the Rayleigh-unstable flows*

In the parameter space, the boundary of the stationary instability (5.13), corresponding to a simple zero root, and the boundary of the Hopf bifurcation (5.15), corresponding to a pair of imaginary roots, may have common codimension-2 points with the coordinates (Pr^*, Ta^*) given for $Ro + 1 < 0$ and $\gamma_a > 0$ by

$$Pr^* = -\frac{1}{2} + \frac{1}{2}\sqrt{1 + 16\frac{(1-\gamma_a\hat{\Theta})}{\gamma_a\hat{\Theta}}\frac{(1+Ro)}{Rt}}, \tag{5.18}$$

$$Ta^* = \frac{1}{\sqrt{2\gamma_a\hat{\Theta}RtPr^* - 4(1-\gamma_a\hat{\Theta})(1+Ro)}}. \tag{5.19}$$

5.5. *The Rayleigh line*

In the particular case $Ro = -1$, corresponding to the Rayleigh line, the roots of the dispersion relation are found explicitly for an arbitrary Pr:

$$\chi_{1,2} = -\frac{Pr+1}{2TaPr} \pm \sqrt{2Rt\hat{\Theta}\gamma_a + \frac{(Pr-1)^2}{4Ta^2Pr^2}}, \quad \chi_3 = -\frac{1}{Ta}. \tag{5.20a,b}$$

One of the first two roots vanishes at the threshold of stationary instability $Ta = Ta_c^S$, where $(\gamma_a < 0, Rt < 0)$

$$Ta_c^S = \frac{1}{\sqrt{2\gamma_a\hat{\Theta}RtPr}}. \tag{5.21}$$

Thus, at the Rayleigh line, stationary instability is possible for inward heating only. When the heating is outward and $Rt < 0$, both the criteria (5.11) and (5.14) are fulfilled and the flow is stable.

6. Stationary and oscillatory modes

The relations (5.13) and (5.15) contain, besides Pr, the group of parameters Ro, $\gamma_a\hat{\Theta}$ and $\gamma_a\hat{\Theta}Rt$, $Rt < 0$. Therefore, the conditions for the occurrence of stationary or oscillatory modes can be analysed in terms of these parameters.

Let us define the Brunt–Väisälä frequency N as Meyer *et al.* (2015) (these authors have defined N^2 with the opposite sign)

$$N^2 = \frac{1}{\rho_0}\nabla\rho \cdot \boldsymbol{g}_{cB} = \frac{1}{\rho_0}\frac{\mathrm{d}\rho}{\mathrm{d}r}\frac{V^2}{r}. \tag{6.1}$$

Taking into account that $\rho(r) = \rho_0(1 - \alpha\theta(r))$ in the Boussinesq approximation, we conclude that $N^2 = -2\gamma_a\hat{\Theta}Rt\,\Omega^2$.

In the diffusionless case, for $Ro < -1$, the flow is Rayleigh unstable, i.e. the radial stratification of the square of the angular momentum is negative; for $Ro > -1$, the flow is Rayleigh stable (Chandrasekhar 1961). The centrifugal acceleration is oriented away from the rotation axis, implying that outward heating ($\gamma_a > 0$) corresponds to a stable stratification of the density ($N^2 > 0$) while inward heating ($\gamma_a < 0$) corresponds to an unstable density stratification, characterized by the negative sign of the squared Brunt–Väisälä frequency ($N^2 < 0$).

For Rayleigh-stable flow configurations, negative stratification of the density yields a thermal instability analogue to Rayleigh–Bénard convection, which might lead to stationary modes at the onset. For Rayleigh-unstable configurations, negative density stratification enforces the centrifugal instability and decreases the threshold compared to the isothermal flow; while positive density stratification will delay the threshold and inertial waves may be excited by the rotation when N^2 becomes significant. These inertial waves, observed in numerical simulations, have been recently reported in Meyer *et al.* (2015).

6.1. *Stationary modes*

Taking into account the relations (4.16) we write the threshold for the onset of stationary instability (5.13) in terms of the parameters of Couette–Taylor flow

$$r_S = \frac{Ta_c^S}{Ta_0} = \left[1 - \frac{\gamma_a}{2} + \frac{\gamma_a Pr}{\ln\eta}(Ta_0)^2\right]^{-1/2}, \tag{6.2}$$

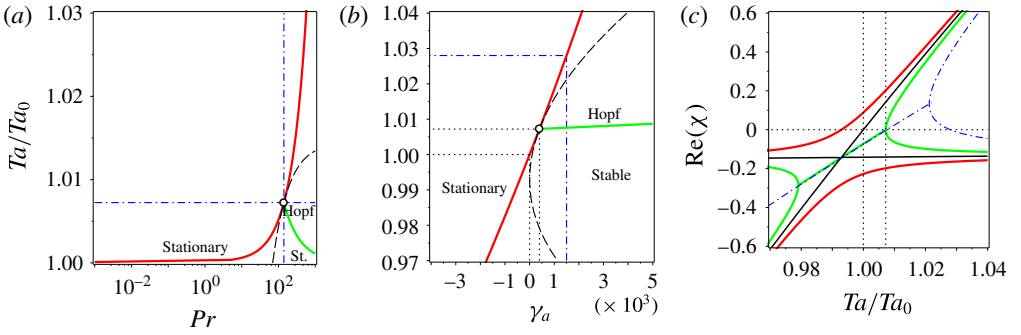

FIGURE 1. (Colour online) Rotating inner cylinder with $\mu = 0$, $\eta = 0.99$. (*a*) Stability diagram at $\gamma_a = 0.0004$ showing the boundaries of stationary instability (6.2) and Hopf bifurcation (6.6) that have a common codimension-2 point ($Pr^* \approx 140.55$, $Ta^*/Ta_0 \approx 1.0072$) given by (6.8) and (6.9). The black dashed line corresponds to double real roots χ: $\chi < 0$ in the stability domain, $\chi > 0$ in the instability domain, and $\chi = 0$ at the codimension-2 point. (*b*) The critical values of Ta/Ta_0 versus γ_a at $Pr \approx 140.55$ with the codimension-2 point ($\gamma_a = 0.0004$, $Ta/Ta_0 \approx 1.0072$) and the (black dashed) line of real eigenvalues. (*c*) Growth rates (Reχ) at $Pr \approx 140.55$ and (red) $\gamma_a = -0.0004$, (black) $\gamma_a = 0$, (green) $\gamma_a = 0.0004$, (dashdot blue) $\gamma_a = 0.0015$.

where we have introduced the threshold for the isothermal flow as follows

$$Ta_c^S(\gamma_a = 0) = \frac{1}{2}\sqrt{\frac{-1}{Ro+1}} \equiv Ta_0. \tag{6.3}$$

For circular Couette flow, the quantity $(Ta_0)^2$ is positive when $Ro + 1 < 0$ (or $\mu < \eta^2$), i.e. in the Rayleigh-unstable zone, and $(Ta_0)^2 < 0$ when $Ro + 1 > 0$, i.e. in the Rayleigh-stable zone (Chandrasekhar 1961). The explicit expressions for Ta_c^S calculated for different rotating regimes of Couette–Taylor flow are given in table 2.

In figure 1 we plot the threshold (6.2) in the Rayleigh-unstable case of the inner cylinder rotation with $\mu = 0$ and $Ro + 1 = -\eta/(1-\eta) < 0$, see table 1. We see that the ratio $r_S < 1$, i.e. there is a destabilization, for inward heating ($\gamma_a < 0$), and $r_S > 1$ for outward heating ($\gamma_a > 0$). Note that the threshold of the stationary modes (6.2) is a function of the parameter $\widehat{S} = -\gamma_a Pr/\ln\eta$, where $|\gamma_a| \ll 1$ in the Boussinesq approximation. This result theoretically justifies the numerical analysis of Meyer *et al.* (2015), where it was shown that the stationary critical modes almost scaled with the temperature drop coefficient $S = \widehat{S}\eta/(1-\eta)$.

Stationary modes can exist if the radicand in (5.13) is positive, this yields a condition on Pr to be satisfied. In the case of Rayleigh-unstable flow, i.e. when $1 + Ro < 0$, the stationary modes exist for any value of Pr when $\gamma_a < 0$ and for $0 \leqslant Pr < Pr^S$ when $\gamma_a > 0$, where the critical value of the Prandtl number is

$$Pr^S = \frac{2(1+Ro)(1-\gamma_a\hat{\Theta})}{\gamma_a\hat{\Theta}Rt}. \tag{6.4}$$

The values of Pr^S calculated in terms of the parameters (4.16) for different rotating cases of the Couette–Taylor system are given in table 1. In the case of the rotating inner cylinder shown in figure 1(*a*) the asymptotic value (6.4) for the threshold (6.2) is $Pr^S \approx 9948$.

	Ta_c^S	Ta_c^H	ω_c/Ω
Rot.			
Inn.	$\left[\dfrac{2\,(2-\gamma_a)\,\eta}{1-\eta}+\dfrac{\gamma_a Pr}{\ln\eta}\right]^{-1/2}$	$\dfrac{1+Pr}{Pr}\left[\dfrac{2(2-\gamma_a)\eta}{1-\eta}+\dfrac{\gamma_a}{2\ln\eta}\dfrac{1+Pr}{Pr}\right]^{-1/2}$	$\dfrac{\beta}{1+Pr}\left[\dfrac{2\eta(\gamma_a-2)}{1-\eta}-\dfrac{\gamma_a Pr(1+Pr)}{2\ln\eta}\right]^{1/2}$
Ray.	$\left[\dfrac{\gamma_a Pr}{\ln\eta}\right]^{-1/2}$		
Sol.	$\left[2(\gamma_a-2)+\dfrac{\gamma_a Pr}{\ln\eta}\right]^{-1/2}$	$\dfrac{1+Pr}{Pr}\left[2(\gamma_a-2)+\dfrac{\gamma_a}{2\ln\eta}\dfrac{1+Pr}{Pr}\right]^{-1/2}$	$\dfrac{\beta}{1+Pr}\left[2(2-\gamma_a)-\dfrac{\gamma_a Pr(1+Pr)}{2\ln\eta}\right]^{1/2}$
Kep.	$\left[\dfrac{2\sqrt{\eta}\,(2-\gamma_a)}{(1+\sqrt{\eta})^2}+\dfrac{\gamma_a Pr}{\ln\eta}\right]^{-1/2}$	$\dfrac{1+Pr}{Pr}\left[\dfrac{2\sqrt{\eta}(2-\gamma_a)}{(1+\sqrt{\eta})^2}+\dfrac{\gamma_a}{2\ln\eta}\dfrac{1+Pr}{Pr}\right]^{-1/2}$	$\dfrac{\beta}{1+Pr}\left[\dfrac{2\sqrt{\eta}(\gamma_a-2)}{(1+\sqrt{\eta})^2}-\dfrac{\gamma_a Pr(1+Pr)}{2\ln\eta}\right]^{1/2}$
Out.	$\left[\dfrac{2\,(2-\gamma_a)}{\eta-1}+\dfrac{\gamma_a Pr}{\ln\eta}\right]^{-1/2}$	$\dfrac{1+Pr}{Pr}\left[\dfrac{2(\gamma_a-2)}{1-\eta}+\dfrac{\gamma_a}{2\ln\eta}\dfrac{1+Pr}{Pr}\right]^{-1/2}$	$\dfrac{\beta}{1+Pr}\left[\dfrac{2(2-\gamma_a)}{1-\eta}-\dfrac{\gamma_a Pr(1+Pr)}{2\ln\eta}\right]^{1/2}$

TABLE 2. Thresholds of the critical modes and the critical Hopf frequency for different rotation regimes in the Couette–Taylor system: (Inn.) inner cylinder rotating, (Ray.) Rayleigh line, (Sol.) solid body rotation, (Kep.) Keplerian rotation, (Out.) outer cylinder rotating.

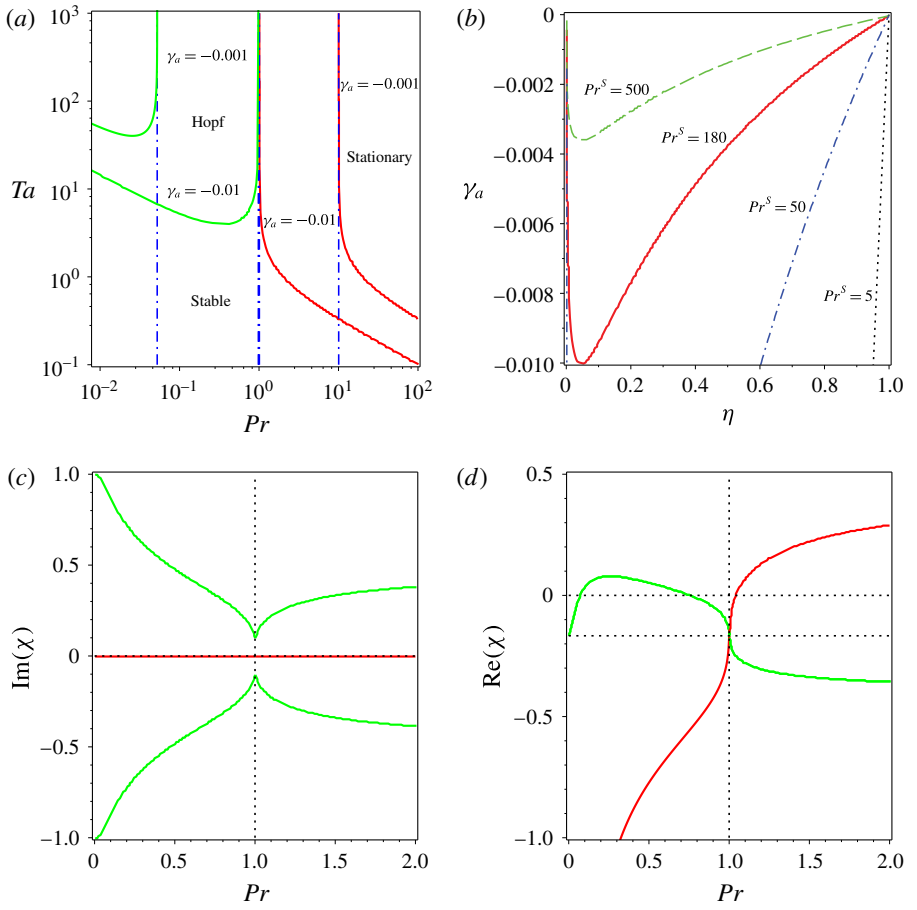

FIGURE 2. (Colour online) Keplerian case with $\mu = \eta^{3/2}$ and $\eta = 0.99$. (*a*) Variation of the threshold of the stationary instability and Hopf bifurcation with Pr at $\gamma_a < 0$ (an inward temperature gradient). The asymptotic values of Pr marked by dot-dashed lines are, respectively: $Pr^H \approx 0.0523$, $Pr^H \approx 0.98$, $Pr^S \approx 1.01$ and $Pr^S \approx 10.055$. (*b*) Lines $Pr^S = \text{const.}$ in the (η, γ_a)-plane. (*c*,*d*) Variation of the frequencies $\text{Im}(\chi)$ and the growth rates $\text{Re}(\chi)$ with Pr at $Ta = 6$ and $\gamma_a = -0.01$ (an inward temperature gradient). The green lines correspond to oscillatory modes, and the red lines to stationary modes.

In the case of Rayleigh-stable flows ($1 + Ro > 0$), the stationary modes are expected only for inward heating ($\gamma_a < 0$) at $Pr > Pr^S$. Figure 2 shows the variation of the threshold with Pr for Keplerian rotation in the small gap case $\eta = 0.99$; the corresponding stability diagrams for the cases of solid body rotation and outer cylinder rotation are shown in figure 3.

Note that for the Rayleigh-unstable flows the stationary modes exist even in the limit of vanishing Prandtl number ($Pr \to 0$), i.e. for highly thermally conducting liquids with low kinematic viscosity. In this limit, the threshold (5.13) reduces to the expression

$$Ta_c^S = \frac{1}{\sqrt{-4(1+Ro)(1-\gamma_a\hat{\Theta})}}. \tag{6.5}$$

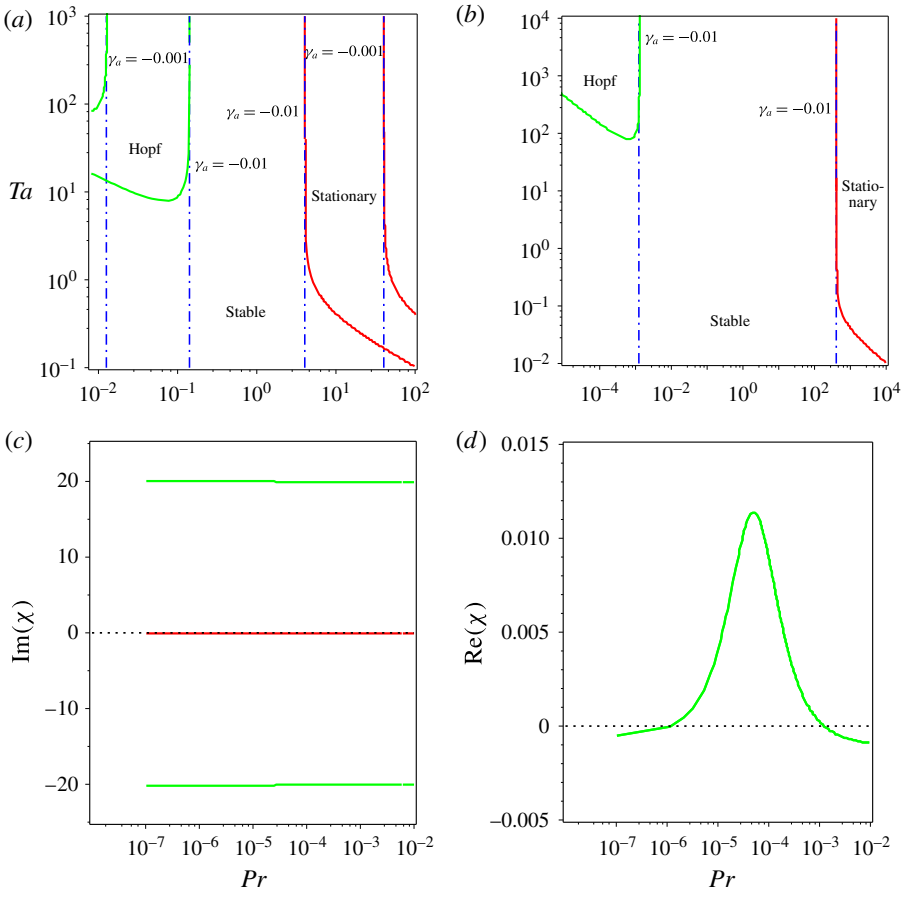

FIGURE 3. (Colour online) (*a*) Solid body rotation with $\mu = 1$ and $\eta = 0.99$. Thresholds of the stationary instability and Hopf bifurcation with the asymptotic values of Pr marked by dot-dashed lines: $Pr^H \approx 0.0126$, $Pr^H \approx 0.1412$, $Pr^S \approx 4.0402$, and $Pr^S \approx 40.221$. (*b*) Outer cylinder rotation with $\mu = \infty$ and $\eta = 0.99$. Thresholds of the stationary instability and Hopf bifurcation with the asymptotic values of the Prandtl number: $Pr^H \approx 0.0012$ and $Pr^S \approx 404.02$. (*c*,*d*) Variation of the (*c*) frequencies and (*d*) growth rates with Pr for outer cylinder rotation ($\mu = \infty$, $\eta = 0.99$) at given $Ta = 1000$ and $\gamma_a = -0.01$. The green lines correspond to the oscillatory modes and the red line corresponds to a (damped) stationary mode.

For Rayleigh-stable flows ($1 + Ro > 0$) the threshold of the stationary modes (5.13) decreases towards zero at $\gamma_a < 0$ in the limit of large values of the Prandtl number ($Pr \to \infty$), i.e. for highly viscous and poorly heat-conducting fluids, see figures 2 and 3.

6.2. *Hopf bifurcation*

In terms of the parameters (4.16) and (6.3) the threshold for the onset of oscillatory instability (5.15) becomes

$$r_H = \frac{Ta_c^H}{Ta_0} = \frac{Pr+1}{Pr}\left[1 - \frac{\gamma_a}{2} + \frac{\gamma_a}{2\ln\eta}\frac{Pr+1}{Pr}\,(Ta_0)^2\right]^{-1/2} \tag{6.6}$$

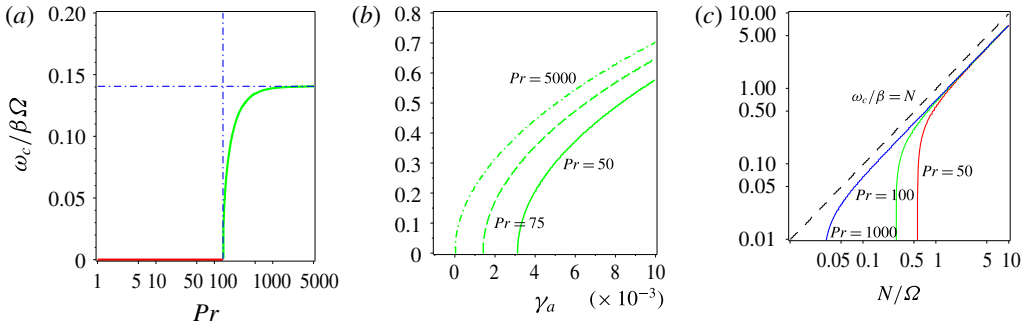

FIGURE 4. (Colour online) Rotating inner cylinder with $\mu = 0$ and $\eta = 0.99$. The critical frequency ω_c at the onset of (red) stationary instability and (green) Hopf bifurcation in units of $\beta\Omega$ (*a*) versus Pr at $\gamma_a = 0.0004$ and (*b*) versus γ_a according to (6.7). The limiting frequency (6.12) at $\gamma_a = 0.0004$ is $(\omega_\infty/\beta\Omega) \approx 0.1411$. (*c*) The critical Hopf frequency ω_c as a function of the Brunt–Väisälä frequency N according to (6.11) and (6.13). The critical frequency vanishes at $N_c/\Omega \approx 0.5572$ for $Pr = 50$, at $N_c/\Omega \approx 0.28$ for $Pr = 100$, and at $N_c/\Omega \approx 0.0281$ for $Pr = 1000$ calculated by means of (6.14) and (4.16).

and the Hopf frequency of the oscillatory modes (5.17) acquires the form

$$\frac{\omega_c}{\Omega} = \frac{\beta}{Pr+1}\frac{1}{Ta_0}\sqrt{-1+\frac{\gamma_a}{2}-\frac{\gamma_a Pr(Pr+1)}{2\ln\eta}\,(Ta_0)^2}. \tag{6.7}$$

Figure 1(*a*,*b*) illustrates the variation of the threshold of Hopf bifurcation with Pr and γ_a for circular Couette flow with the inner cylinder rotating alone. The variation of the Hopf frequency with Pr and γ_a in this rotating case is shown in figure 4. Similarly to stationary instability, both the threshold (6.6) and the frequency (6.7) of the oscillatory modes depend explicitly on the Prandtl number Pr and on the temperature drop parameter $\widehat{S}$, in agreement with the numerical calculations of (Meyer *et al.* 2015).

We see that at $\gamma_a > 0$ both $r_H > 1$ and $r_S > 1$, i.e. outward heating is stabilizing for both stationary and oscillatory modes with respect to isothermal flow. The growth rates shown in figure 1(*c*) demonstrate that the complex roots do not exist at $\gamma_a \leqslant 0$; they appear at $\gamma_a > 0$ due to splitting of a double real eigenvalue. When this eigenvalue is negative the complex roots are stable. They acquire a positive growth rate only after a double real eigenvalue passes through zero with the change of parameters, which happens exactly at a codimension-2 point, cf. Tuckerman (2001).

Indeed, since this flow is Rayleigh-unstable in the absence of diffusion, the branches of the stationary and oscillatory modes have a common codimension-2 point with the coordinates (5.18) and (5.19) that in the parametric representation, (4.16) and (6.3) can be written as follows:

$$Pr^* = -\frac{1}{2}+\frac{1}{2}\sqrt{1-4\frac{2-\gamma_a}{\gamma_a}\frac{\ln\eta}{(Ta_0)^2}}, \tag{6.8}$$

$$Ta^* = Ta_0\left[1-\frac{\gamma_a}{2}+\gamma_a Pr^*\frac{(Ta_0)^2}{\ln\eta}\right]^{-1/2}. \tag{6.9}$$

At the codimension-2 point one of the roots of the dispersion relation is double zero and the other one is simple real and negative, corresponding to a damped mode, as the growth rates demonstrate in figure 1(*c*).

The threshold for the excitation of oscillatory modes and the corresponding critical frequency of the oscillatory modes for both the Rayleigh-stable and the Rayleigh-unstable rotation regimes in the Couette–Taylor system are summarized in table 2. For the Rayleigh-unstable flows with outward heating the oscillatory instability actually occurs at $Pr > Pr^*$, where Pr^* is given by (5.18) or (6.8), see figure 1.

Figures 2 and 3 show the boundaries of stationary instability and Hopf bifurcation in the (Pr, Ta)-plane for Rayleigh-stable flows such as Keplerian rotation, solid-body rotation and the case of the outer cylinder rotating. We see also that the frequency of the oscillatory instability is increasing while approaching the outer cylinder rotating case, whereas the growth rate of the oscillatory instability at low Pr is decreasing.

All these Rayleigh-stable flows ($1 + Ro > 0$ or $\mu \geqslant \eta^2$) with inward heating ($\gamma_a < 0$) share the same property. Namely, the oscillatory modes are excited when thermal diffusion dominates over the fluid viscosity

$$0 < Pr < Pr^H = \frac{\gamma_a \hat{\Theta} Rt}{\gamma_a \hat{\Theta} Rt - 4(1+Ro)(1-\gamma_a \hat{\Theta})} < 1. \tag{6.10}$$

This result follows from the observation that the Hopf bifurcation from the base flow can occur if the radicand in (5.15) is positive. In contrast, the stationary modes are excited in the Rayleigh-stable flow by inward heating when $Pr > Pr^S > 1$, where Pr^S is given in (6.4) and table 1.

Therefore, for Rayleigh-stable flows an inward radial temperature gradient destabilizes the flow depending on the value of Pr. The oscillatory instability occurs at $0 < Pr < 1$ while the stationary instability takes place at $Pr > 1$. At $Pr = 1$ the flows remain stable, becoming unstable only when $Pr \neq 1$, which is a characteristic feature of double-diffusive instabilities (Acheson & Gibbons 1978; Kirillov & Verhulst 2010; Kirillov 2013).

As figures 2 and 3 demonstrate, when $Pr \to 0$, the threshold of the oscillatory modes (5.15) occurring in the Rayleigh-stable flows becomes infinite ($Ta_c^H \to \infty$) while their frequency $\bar{\omega}_c \to 2\sqrt{(1+Ro)(1-\gamma_a\hat{\Theta})}$ depends weakly on the heating parameter γ_a.

The opposite limit, when $Pr \to \infty$, is applicable to the threshold of Hopf bifurcation in Rayleigh-unstable flows with outward heating ($\gamma_a > 0$), yielding $Ta_c^H \to [\gamma_a \hat{\Theta} Rt - 4(1-\gamma_a\hat{\Theta})(1+Ro)]^{-1/2}$. The corresponding Hopf frequency becomes independent of the rotation rate: $\bar{\omega}_\infty = \sqrt{-\gamma_a \hat{\Theta} Rt}$, as is visible in figure 4(*a*). Figure 4(*b*) shows that the Hopf frequency is bounded ($0 < \bar{\omega}_c < \bar{\omega}_\infty$) at any fixed $Pr^* < Pr < \infty$.

The frequency $\bar{\omega}_\infty$ is fixed by the Brunt–Väisälä frequency N in the case of stable stratification of the fluid density ($\gamma_a > 0$, $Rt < 0$), as is evident in figure 4(*c*). Indeed, for a fixed value of Pr, the Hopf frequency (5.17) can be expressed via the Brunt–Väisälä frequency as

$$\bar{\omega}_c = \sqrt{\frac{N^2}{2\Omega^2}\frac{Pr}{Pr+1} + \frac{4(1+Ro)(1-\gamma_a\hat{\Theta})}{(Pr+1)^2}}. \tag{6.11}$$

Hence, in the limit of $Pr \to \infty$ we have

$$\bar{\omega}_\infty = \frac{1}{\sqrt{2}}\frac{N}{\Omega} = \sqrt{-\frac{\gamma_a}{2\ln\eta}}, \tag{6.12}$$

which, in particular, yields another expression for the Brunt–Väisälä frequency in the case of Rayleigh-unstable flows with outward heating ($\gamma_a > 0$):

$$N^2 = -\frac{\gamma_a}{\ln \eta}\Omega^2. \tag{6.13}$$

Figure 4(*c*) shows that all the critical frequencies tend asymptotically to the line (6.12) as $N/\Omega \to \infty$. With a decrease in the ratio N/Ω the critical frequency vanishes at the characteristic value of the Brunt–Väisälä frequency N_c given by

$$\frac{N_c^2}{\Omega^2} = -\frac{8(1+Ro)(1-\gamma_a\hat{\Theta})}{Pr(Pr+1)}. \tag{6.14}$$

The characteristic Brunt–Väisälä frequency N_c determines the stratification that is required to excite inertial waves by the rotation. Since N_c decreases with an increase in Pr (figure 4), we conclude that the inertial waves are easier to excite in Rayleigh-unstable flow by an outward radial temperature gradient in the case of highly viscous fluids than in the case of weakly viscous fluids.

7. Discussion

The short-wavelength approximation has been used to investigate the stability of Taylor–Couette flow with a radial buoyancy force induced by coupling between a radial temperature gradient and the centrifugal force in the Boussinesq approximation. A characteristic polynomial equation has been analysed and marginal stability branches of stationary and oscillatory modes have been found analytically. The present method allows one to find the explicit dependence of the marginal state with the main control parameters: Pr, Ro, γ_a and Rt.

The reader should be aware that for the validity of the Boussinesq approximation, the thermal expansion parameter must be very small (i.e. $|\gamma_a| \ll 1$) so that it is possible to neglect γ_a before 1 in all expressions containing $1 - \gamma_a/2$. In fact, in our computations, the largest value of $|\gamma_a|$ was $|\gamma_a| = 0.01$ for fluids with the largest expansion coefficient found in the literature, to which a maximum of temperature difference applied should not exceed $\Delta T_{max} = 5\,^{\circ}\mathrm{C}$.

From the above results computed at the geometric mean radius, for each value of rotating case in circular Couette flow (i.e. for a given value of μ), it is possible to determine the critical modes and their threshold Ta_c as a function of different flow parameters η, γ_a and Pr together with the critical frequency for oscillatory modes. We have determined the critical parameters for the particular case of specific interest: sole inner cylinder rotation ($\mu = 0$), sole outer cylinder rotation ($\mu \to \infty$), solid body rotation ($\mu = 1$) and Keplerian rotation ($\mu = \eta^{3/2}$).

For the inner cylinder sole rotation, we have retrieved and extended the results of linear stability analysis (Meyer *et al.* 2015). For example, we have proved easily that the slope of the branch of stationary modes at the origin ($\gamma_a = 0$) is increasing with both Pr and η. In fact, one gets

$$\frac{\mathrm{d}Ta}{\mathrm{d}\gamma_a}(\gamma_a = 0) = \frac{Ta_0}{4}\left(1 - \frac{2Pr(Ta_0)^2}{\ln \eta}\right). \tag{7.1}$$

To our best knowledge, Rayleigh-stable flows (except solid body rotation) with a radial temperature gradient have never been treated analytically in such detail so far

and the results presented in this work offer new predictions of convective instabilities. In the case of sole outer cylinder rotation, in the case of solid body rotation, and in the Keplerian regime, inward heating is destabilizing and leads to the oscillatory instability via Hopf bifurcation at $0 < Pr < Pr^H < 1$ and to stationary instability for any value $Pr > Pr^S > 1$, where the thresholds depend on γ_a and η (table 1). The values of Pr for which the oscillatory instability is observed are comparable to those of the astrophysical flows for which $Pr \approx 0.02$. At the Rayleigh line the flow is unstable for inward heating. The present model is based on the short-wavelength approximation in the axial direction, so, strictly speaking, it cannot be applied as such to the case of solid body rotation, where it is known (Auer, Busse & Clever 1995) that the critical modes are columnar vortices ($n \neq 0, k = 0$).

In appendix A we have compared the present results with those derived by Economides and Moir (Economides & Moir 1980) for Taylor–Couette flow with a centripetal acceleration and a radial temperature gradient. Lopez *et al.* (2013) have investigated the stability of a rotating cylindrical annulus with a negative radial temperature gradient and in the presence of gravity g. While these authors suggested that quasi-Keplerian flows may be stable for weak stratification in the radial direction, our results show that laminar quasi-Keplerian flows may be destabilized by the centrifugal buoyancy, leading to oscillatory modes for values of Pr relevant to accretion-disc problem, although we have considered a model that has solid radial boundaries.

8. Conclusion

The short-wavelength approximation method has been applied to the linear stability of circular Couette flow with a centrifugal buoyancy induced by a radial temperature gradient in the absence of natural gravity. The marginal states (stationary and oscillatory modes) have been determined analytically and the effects of the different parameters of the problem on flow stability have been analysed in detail. The centrifugal buoyancy enhances the instability of Rayleigh-unstable flows in inward heating, and in outward heating it induces oscillatory modes, the frequency of which can be compared with the Brunt–Väisäla frequency in the limit of large Pr values. In inward heating it also induces instability in Rayleigh-stable flows in the form of stationary modes for large values of Pr or oscillatory modes for small values of Pr. The present study may serve as a theoretical guideline to linear stability analysis and to direct numerical simulations (DNS) of the flow.

Acknowledgements

O.N.K. has benefited from the CNRS grant for visiting senior scholars and acknowledges financial support from the ERC Advanced Grant 'Instabilities and nonlocal multiscale modelling of materials' FP7-PEOPLE-IDEAS-ERC-2013-AdG (2014-2019). I.M. is grateful to A. Meyer and Y. Harunori and O.N.K. is grateful to L. Tuckerman for fruitful exchanges on this work. I.M. acknowledges support from the French National Research Agency (ANR) through the program Investissements d'Avenir (No. ANR-10 LABX-09-01), LABEX EMC^3 (project TUVECO) and from the CPER Normandie.

Appendix A. Link to Economides & Moir (1980)

In the appendix we would like to compare our short-wavelength equations with the matrix (4.6) to the results by Economides and Moir (Economides & Moir 1980) derived in the narrow-gap approximation.

Let $d = R_2 - R_1 \ll R_1$ be the size of the gap between the cylinders in the Couette cell. Then, we can write

$$x = (r - R_1)/d, \quad \mu = \Omega_2/\Omega_1, \quad \Omega(x) = 1 - (1-\mu)x, \quad x \in [0, 1]. \tag{A 1a–d}$$

Denoting $D = \mathrm{d}/\mathrm{d}x$ so that $\mathrm{d}/\mathrm{d}r = d^{-1}\mathrm{d}/\mathrm{d}x$ we define the operators

$$\left.\begin{aligned} L &= D^2 - (k_z d)^2 - \sigma - \mathrm{i}k\sqrt{T}\Omega(x), \\ M &= D^2 - (k_z d)^2 - \sigma Pr - \mathrm{i}kPr\sqrt{T}\Omega(x), \end{aligned}\right\} \tag{A 2}$$

where $Pr = \nu/\kappa$ is the Prandtl number and

$$\sigma = \frac{\omega d^2}{\nu}, \quad k = m\sqrt{-\frac{\Omega_1}{4A}}, \quad T = -\frac{4A\Omega_1 d^4}{\nu^2}, \quad \bar{\beta} = \frac{T_2 - T_1}{R_2 - R_1}. \tag{A 3a–d}$$

The temporal eigenvalue is denoted by ω and the azimuthal wavenumber by m. The parameter A is a coefficient in the expression for the background circular Couette flow

$$r\Omega(r) = Ar + \frac{B}{r} \tag{A 4}$$

and can be expressed via the Rossby number Ro as Kirillov *et al.* (2014):

$$A = \Omega(1 + Ro). \tag{A 5}$$

Then, the system of the narrow-gap equations derived in Economides & Moir (1980) is

$$\left.\begin{aligned} L(D^2 - (k_z d)^2)u' &= -(k_z d)^2 T\Omega(x)v' + (k_z d)^2 R\theta', \\ Lv' &= u', \\ M\theta' &= u', \end{aligned}\right\} \tag{A 6}$$

where (with g denoting constant gravitational acceleration and α the coefficient of thermal expansion)

$$R = \frac{g\alpha\bar{\beta}d^4}{\nu\kappa}, \quad u' = \frac{2Ad\delta}{\nu\Omega_1}u, \quad v' = \frac{v}{R_1\Omega_1}, \quad \theta' = \frac{2A\kappa\theta}{\bar{\beta}\nu\Omega_1 R_1}, \quad \delta = \frac{d}{R_1}. \tag{A 7a–e}$$

For any $w \sim \exp(\mathrm{i}k_r r)$, we have

$$\begin{aligned} Lw &= -\frac{d^2}{\nu}[\nu(k_r^2 + k_z^2) + \omega + \mathrm{i}m\Omega_1\Omega(x)]w \\ &= -\frac{d^2}{\nu}[\nu|\boldsymbol{k}|^2 + \omega + \mathrm{i}m\Omega_1\Omega(x)]w \\ &= -\frac{d^2}{\nu}[\omega_\nu + \omega + \mathrm{i}m\Omega_1\Omega(x)]w. \end{aligned} \tag{A 8}$$

Hence, if $u, v \sim \exp(\mathrm{i}k_r r)$ the first of (A 6) becomes

$$\begin{aligned} &-\frac{d^2}{\nu}\left[\omega_\nu + \omega + \mathrm{i}m\Omega_1\Omega(x)\right](-d^2|\boldsymbol{k}|^2)\frac{2Ad\delta}{\nu\Omega_1}u \\ &\quad = -(k_z d)^2(-4A\Omega_1 d^4)\frac{\Omega(x)}{\nu^2 R_1\Omega_1}v + (k_z d)^2\frac{2Ag\alpha d^4}{\nu^2\Omega_1 R_1}\theta. \end{aligned} \tag{A 9}$$

Simplifying the above expression, we find

$$[\omega_\nu + \omega + \mathrm{i}m\Omega_1\Omega(x)]\, u = \frac{k_z^2}{|\boldsymbol{k}|^2} 2\Omega_1\Omega(x)\frac{d}{\delta R_1} v + \frac{k_z^2}{|\boldsymbol{k}|^2}\frac{d}{\delta R_1} g\alpha\theta \tag{A 10}$$

and finally

$$[\omega_\nu + \omega + \mathrm{i}m\Omega_1\Omega(x)]\, u = \frac{k_z^2}{|\boldsymbol{k}|^2} 2\Omega_1\Omega(x) v + \frac{k_z^2}{|\boldsymbol{k}|^2} g\alpha\theta, \tag{A 11}$$

where $\omega_\nu = \nu|\boldsymbol{k}|^2$.

Analogously, the second of (A 6) becomes

$$-\frac{d^2}{\nu R_1\Omega_1}[\omega_\nu + \omega + \mathrm{i}m\Omega_1\Omega(x)]\, v = \frac{2Ad\delta}{\nu\Omega_1} u. \tag{A 12}$$

Simplifying it, we get

$$[\omega_\nu + \omega + \mathrm{i}m\Omega_1\Omega(x)]\, v = -2Au \tag{A 13}$$

and, finally

$$[\omega_\nu + \omega + \mathrm{i}m\Omega_1\Omega(x)]\, v = -2\Omega(1 + Ro)u. \tag{A 14}$$

Now, for the third of (A 6) we find

$$\left[-k_r^2 d^2 - (k_z d)^2 - \sigma Pr - \mathrm{i}kPr\sqrt{T}\Omega(x)\right] \frac{2A\kappa}{\bar{\beta}\nu\Omega_1 R_1}\theta = \frac{2Ad\delta}{\nu\Omega_1} u, \tag{A 15}$$

and equivalently,

$$\left[-\kappa k_r^2 - \kappa k_z^2 - \omega - \mathrm{i}m\Omega_1\Omega(x)\right] \frac{d}{\bar{\beta}\nu R_1}\theta = \frac{\delta}{\nu} u, \tag{A 16}$$

so that finally

$$[\omega_\kappa + \omega + \mathrm{i}m\Omega_1\Omega(x)]\,\theta = -\bar{\beta} u, \tag{A 17}$$

where $\omega_\kappa = \kappa|\boldsymbol{k}|^2$.

We can denote $\Omega = \Omega_1\Omega(x)$ and write the three equations in the matrix form

$$\begin{pmatrix} \omega_\nu + \omega + \mathrm{i}m\Omega & -\frac{k_z^2}{|\boldsymbol{k}|^2} 2\Omega & -\frac{k_z^2}{|\boldsymbol{k}|^2} g\alpha \\ 2\Omega(1 + Ro) & \omega_\nu + \omega + \mathrm{i}m\Omega & 0 \\ \bar{\beta} & 0 & \omega_\kappa + \omega + \mathrm{i}m\Omega \end{pmatrix} \begin{pmatrix} u \\ v \\ \theta \end{pmatrix} = 0. \tag{A 18}$$

In fact, $\bar{\beta} = (T_2 - T_1)/(R_2 - R_1)$ is a 'derivative' of the temperature with respect to radius and in the local approximation we can replace it with $\Theta' = \mathrm{d}\theta_0/\mathrm{d}r$. Then, we can denote $\beta = (k_z/|\boldsymbol{k}|)$ and write

$$\begin{pmatrix} \omega_\nu + \omega + \mathrm{i}m\Omega & -2\Omega\beta^2 & -\alpha g\beta^2 \\ 2\Omega(1 + Ro) & \omega_\nu + \omega + \mathrm{i}m\Omega & 0 \\ \Theta' & 0 & \omega_\kappa + \omega + \mathrm{i}m\Omega \end{pmatrix} \begin{pmatrix} u \\ v \\ \theta \end{pmatrix} = 0. \tag{A 19}$$

For the stationary axisymmetric instability the Bilharz criterion (Bilharz 1944) applied to the characteristic polynomial of the matrix on the left-hand side of (A 19) yields:

$$4(Ro+1)+Pr\frac{g}{\Omega^2}\frac{2Rt\Theta\alpha}{r}+\frac{1}{Ta^2}>0 \tag{A 20}$$

With $g=\Omega^2 r$, and taking into account that the sign of α in Economides & Moir (1980) is opposite to the sign of α in (2.1), we reduce the above equation to the form

$$4(Ro+1)-2PrRt\hat{\Theta}\gamma_a+\frac{1}{Ta^2}>0, \tag{A 21}$$

which differs from the condition (5.11) only by the factor $1-\gamma_a\hat{\Theta}$ at the first term. The reason for this discrepancy is that in Economides & Moir (1980) g is assumed to be a constant radial gravitational acceleration whereas in Meyer *et al.* (2015) it is the centrifugal acceleration that depends on radius. Hence, substitution of $g=\Omega^2 r$ into (A 20) is not justified. On the other hand, the factor $1-\gamma_a\hat{\Theta}$ is small in the Boussinesq approximation, and consequently (5.11) and (A 21) can be considered as equivalent.

Taking into account that in the Boussinesq approximation the squared Brunt–Väisälä frequency is $N^2=-2\gamma_a\hat{\Theta}Rt\Omega^2$, we transform (A 21) as

$$4(Ro+1)+Pr\frac{N^2}{\Omega^2}+\frac{1}{Ta^2}>0. \tag{A 22}$$

With the opposite sign the inequality (A 22) is the onset of the double-diffusive Goldreich–Schubert–Fricke instability in the form derived in Acheson & Gibbons (1978).

REFERENCES

ACHESON, D. J. & GIBBONS, M. P. 1978 On the instability of toroidal magnetic fields and differential rotation in stars. *Phil. Trans. R. Soc. Lond.* A **289** (1363), 459–500.

ALI, M. & WEIDMAN, P. D. 1990 On the stability of circular Couette flow with radial heating. *J. Fluid Mech.* **220**, 53–84.

ALLILUEVA, A. I. & SHAFAREVICH, A. I. 2015 Asymptotic solutions of linearized Navier–Stokes equations localized in small neighborhoods of curves and surfaces. *Russ. J. Math. Phys.* **22** (4), 421–436.

AUER, M., BUSSE, F. H. & CLEVER, R. M. 1995 Three-dimensional convection driven by centrifugal buoyancy. *J. Fluid Mech.* **301**, 371–382.

BALBUS, S. A. & POTTER, W. J. 2016 Surprises in astrophysical gasdynamics. *Rep. Prog. Phys.* **79**, 066901.

BILHARZ, H. 1944 Bemerkung zu einem Satze von Hurwitz. *Z. Angew. Math. Mech.* **24** (2), 77–82.

CHANDRASEKHAR, S. 1961 *Hydrodynamic and Hydromagnetic Stability*. Clarendon.

CHILD, A., KERSALÉ, E. & HOLLERBACH, R. 2015 Nonaxisymmetric linear instability of cylindrical magnetohydrodynamic Taylor–Couette flow. *Phys. Rev.* E **92**, 033011.

DOBROKHOTOV, S. YU. & SHAFAREVICH, A. I. 1992 Parametrix and the asymptotics of localized solutions of the Navier–Stokes equations in R3, linearized on a smooth flow. *Math. Notes* **51** (1), 47–54.

DUBRULLE, B., DAUCHOT, O., DAVIAUD, F., LONGARETTI, P.-Y., RICHARD, D. & ZAHN, J.-P. 2005 Stability and turbulent transport in Taylor–Couette flow from analysis of experimental data. *Phys. Fluids* **17**, 095103.

ECKHARDT, B. & YAO, D. 1995 Local stability analysis along Lagrangian paths. *Chaos, Solitons Fractals* **5** (11), 2073–2088.

ECKHOFF, K. S. 1981 On stability for symmetric hyperbolic systems, I. *J. Differ. Equ.* **40** (1), 94–115.

ECONOMIDES, D. G. & MOIR, G. 1980 Taylor vortices and the Goldreich–Schubert instability. *Geophys. Astrophys. Fluid Dyn.* **16** (1), 299–317.

FRIEDLANDER, S. & VISHIK, M. M. 1995 On stability and instability criteria for magnetohydrodynamics. *Chaos* **5** (2), 416–423.

KIRILLOV, O. N. 2013 *Nonconservative Stability Problems of Modern Physics*. De Gruyter.

KIRILLOV, O. N. 2016 Singular diffusionless limits of double-diffusive instabilities in magnetohydrodynamics. *Proc. R. Soc. Lond.* A (submitted), arXiv:1610.06970v1.

KIRILLOV, O. N. & STEFANI, F. 2013 Extending the range of the inductionless magnetorotational instability. *Phys. Rev. Lett.* **111**, 061103.

KIRILLOV, O. N., STEFANI, F. & FUKUMOTO, Y. 2014 Local instabilities in magnetized rotational flows: a short-wavelength approach. *J. Fluid Mech.* **760**, 591–633.

KIRILLOV, O. N. & VERHULST, F. 2010 Paradoxes of dissipation-induced destabilization or who opened Whitney's umbrella? *Z. Angew. Math. Mech.* **90** (6), 462–488.

KUCHERENKO, V. V. & KRYVKO, A. 2013 Interaction of Alfvén waves in the linearized system of magnetohydrodynamics for an incompressible ideal fluid. *Russ. J. Math. Phys.* **20** (1), 56–67.

LAPPA, M. 2012 *Rotating Thermal Flows in Natural and Industrial Processes*. Wiley.

LIFSCHITZ, A. 1991 Short wavelength instabilities of incompressible three-dimensional flows and generation of vorticity. *Phys. Lett.* A **157** (8), 481–487.

LIFSHITZ, A. E. 1987 Continuous spectrum in general toroidal systems (ballooning and Alfvén modes). *Phys. Lett.* A **122** (6), 350–356.

LIFSCHITZ, A. & HAMEIRI, E. 1991 Local stability conditions in fluid dynamics. *Phys. Fluids* A **3** (11), 2644–2651.

LIFSCHITZ, A. & HAMEIRI, E. 1993 Localized instabilities of vortex rings with swirl. *Commun. Pure Appl. Maths* **46** (10), 1379–1408.

LIFSCHITZ, A., SUTERS, W. H. & BEALE, J. T. 1996 The onset of instability in exact vortex rings with swirl. *J. Comput. Phys.* **129** (1), 8–29.

LOPEZ, J. M., MARQUES, F. & AVILA, M. 2013 The Boussinesq approximation in rapidly rotating flows. *J. Fluid Mech.* **737**, 56–77.

MARCUS, P. S., PEI, S., JIANG, C.-H. & HASSANZADEH, P. 2013 Three-dimensional vortices generated by self-replication in stably stratified rotating shear flows. *Phys. Rev. Lett.* **111**, 084501.

MASLOV, V. P. 1986 Coherent structures, resonances, and asymptotic non-uniqueness for Navier–Stokes equations with large Reynolds numbers. *Russ. Math. Surveys* **41** (6), 23–42.

MEYER, A., YOSHIKAWA, H. N. & MUTABAZI, I. 2015 Effect of the radial buoyancy on a circular Couette flow. *Phys. Fluids* **27** (11), 114104.

MUTABAZI, I. & BAHLOUL, A. 2002 Stability analysis of a vertical curved channel flow with a radial temperature gradient. *Theor. Comput. Fluid Dyn.* **16** (1), 79–90.

NELSON, R. P., GRESSEL, O. & UMURHAN, O. M. 2013 Linear and non-linear evolution of the vertical shear instability in accretion discs. *Mon. Not. R. Astron. Soc.* **435** (3), 2610–2632.

STEFANI, F. & KIRILLOV, O. N. 2015 Destabilization of rotating flows with positive shear by azimuthal magnetic fields. *Phys. Rev.* E **92**, 051001.

TUCKERMAN, L. S. 2001 Thermosolutal and binary fluid convection as a 2×2 matrix problem. *Physica* D **156**, 325–363.

URPIN, V. & BRANDENBURG, A. 1998 Magnetic and vertical shear instabilities in accretion discs. *Mon. Not. R. Astron. Soc.* **294** (3), 399–406.

VINBERG, E. B. 2003 *A Course in Algebra*. American Mathematical Society.

YOSHIKAWA, H. N., NAGATA, M. & MUTABAZI, I. 2013 Instability of the vertical annular flow with a radial heating and rotating inner cylinder. *Phys. Fluids* **25** (11), 114104.